Laminar flow in a porous channel with large wall suction and a weakly oscillatory pressure

Todd A. Jankowski and Joseph Majdalani[a)]
Department of Mechanical & Industrial Engineering, Marquette University, Milwaukee, Wisconsin 53233

(Received 19 January 2001; accepted 29 November 2001)

The laminar oscillatory flow inside a rectangular channel with wall suction is considered here. The scope is limited to large suction imposed uniformly along the permeable walls. Inside the channel, the onset of small amplitude pressure disturbances produces an oscillatory field that we wish to investigate. Based on the normalized pressure-wave amplitude, the conservation equations are linearized and split into leading-order (steady) and first-order (time-dependent) equations. The first-order set is subdivided into an acoustic, pressure-driven, wave equation, and a vortical, boundary-driven, viscous equation. For longitudinal pressure oscillations, both equations are written to the order of the wall suction Mach number. The resulting equations are then solved in an exact fashion. The novelty lies in the vortical response that reduces to a Weber equation following a Liouville–Green transformation. The emerging rotational solution is expressible in terms of confluent hypergeometric functions of the suction Reynolds number, Strouhal number, and spatial coordinates. The total solution is then constructed and found to coincide with the numerical solution of the linearized momentum equation. The oscillatory velocity exhibits similar characteristics to the exact Stokes profile for oscillations inside a long channel with hard walls. In particular, a thin rotational layer is observed in addition to the small velocity overshoot near the wall. Both depth and overshoot are nowhere near their values obtained by switching from mass extraction to mass addition. In contrast to former studies involving injection, the so-called acoustic boundary layer is found to depreciate when suction is increased or when viscosity is reduced. This response is similar to that of the Stokes layer over hard walls. Overall, the effect of increasing frequency is that of compressing the rotational layer near the wall. © *2002 American Institute of Physics.* [DOI: 10.1063/1.1445419]

I. INTRODUCTION

The focus of this paper is to obtain an analytical solution to the oscillatory velocity field in a porous channel with uniform wall suction. The scope is limited to the large suction case for which an exact solution can be obtained for both pressure-driven and boundary-driven temporal velocities. The work is hoped to increase our understanding of oscillatory and pulsatory flows in porous channels and tubes. Such flows arise in the modeling of the respiratory function in lungs and airways, in the design of hydraulic line transmissions, in sweat cooling, and in boundary-layer control. Since oscillatory flows with wall injection have already been analyzed in former studies,[1] the current article focuses on the wall suction case. Another purpose for this study is to serve as a prelude for a generalized formulation that could be applied to oscillatory flow problems with arbitrary levels of suction.

Much work has been invested in the past for the treatment of nonoscillatory flows in channels with the same geometry considered here. Throughout these studies, numerical, exact or asymptotic mean flow solutions are obtained for different levels of suction or injection along the walls. These formulations stem from a single, nonlinear, fourth-order, ordinary differential equation (ODE) that is an exact solution to the Navier–Stokes equations. The fundamental similarity equation was originally derived by Berman[2] in his analysis of flows that are bounded by porous surfaces. It depends on the cross-flow Reynolds number ($R \equiv v_w h/\nu$) that is based on the wall suction velocity v_w and the channel's half height h. In fact, Berman's landmark paper[2] has set the stage to extensive porous channel flow studies. While some were concerned with developing analytical or numerical mean flow solutions over different ranges of suction (or injection), others have addressed issues regarding solution multiplicity and stability.

With regards to suction flows in rectangular channels, Berman was first in using asymptotic tools to solve the steady flow problem for the small suction case.[2] Soon thereafter, Yuan,[3] Sellars,[4] and Terrill[5] developed solutions that extended over increasingly larger ranges of suction. For example, Yuan[3] extended Berman's range to $R=20$, and Sellars[4] produced one exact solution for $R\to\infty$. For large suction, Terrill[5] presented an asymptotic solution that contained viscous corrections of order R^{-1}. As $R\to\infty$, Terrill's leading-order term reproduced Sellars' exact solution for infinite suction. Note that later studies have indicated that three total solutions could exist for large R.[6–11] In fact, according to Zaturska, Drazin, and Banks,[8] three types of symmetric

a)Telephone: (414) 288-6877; Fax (414) 288-7790. Electronic mail: maji@mu.edu

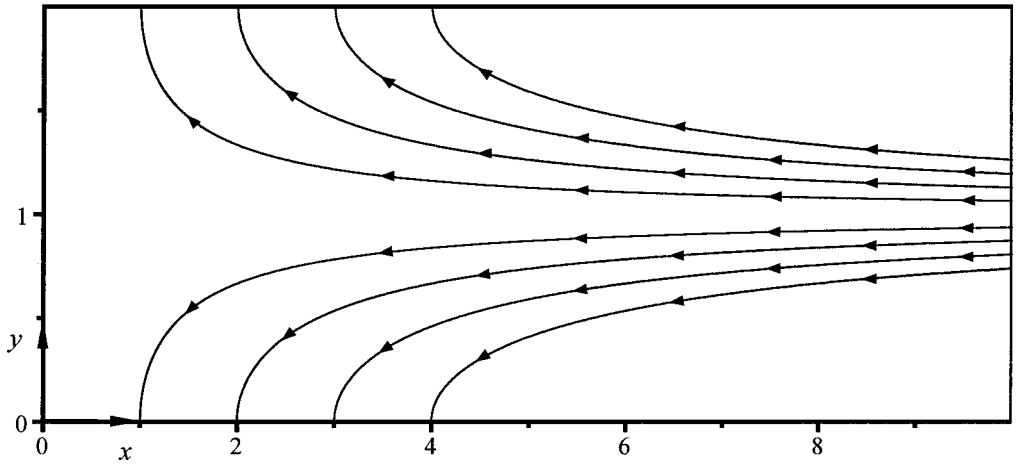

FIG. 1. System geometry showing select mean flow streamlines.

solutions exist in separate intervals covering the entire range for suction. The three solutions are described as an increasing concave down function, an increasing function with a reflection point, and a nonmonotone function with a turning point. These three solutions are referred to as types I, II, and III, respectively. As $R\to\infty$, solutions of type I and II share the same leading order linear term that is used in the current analysis (cf. Zaturska, Drazin, and Banks,[8] p. 165). The type III solution, however, is trigonometric in nature. It was first alluded to by Robinson[6] and further verified independently by MacGillivray and Lu,[7] and Zaturska, Drazin and Banks.[8] It has been finally illuminated in two contemporaneous articles by Cox and King,[10] and Lu.[11] These recent studies have provided rigorous descriptions of the mean flow field arising from the type III branch. Of the steady symmetric solutions, only the type I branch has been shown to be temporally stable for $R<6.001\,353$. For large R, all three solutions are unstable to disturbances of similarity form. For this reason, it has been speculated that these solutions are unlikely to be reproducible in practice. Yet no experimental data is available to either confirm or deny their physicality. In this article, we have made the tacit assumption that the leading order part of types I and II can be a representative model of the mean flow field. This enables us to extract an exact solution, be it academic, for the rotational disturbances. In a later study, we hope to address the same problem with the type III solution serving to describe the mean flow motion. In that case, only asymptotic solutions will be shown to exist following a careful application of perturbation tools.

It should be noted that former mean flow studies have not considered possible fluctuations in the wall suction rate. Such fluctuations can be inevitable and take place at random frequencies. Those matching the channel's natural frequencies can be amplified to the point of promoting a self-sustaining acoustic field. The oscillatory pressure disturbances that are thus produced can give rise to acoustic velocity oscillations that alter the mean flow character. The velocity oscillations stem from both acoustic (pressure-driven) and vorticity (boundary-driven) disturbance modes.[12] Since no other study seems to have explored the resulting temporal field, it is the purpose of this article to find an analytical solution that can be used to characterize the self-induced oscillatory field in a channel with large wall suction. For cases that involve externally induced motion (as opposed to self-triggered oscillations), the same analysis presented here may be employed.

The mathematical modeling starts in Sec. II with a definition of the system geometry. This is followed by a listing of pertinent assumptions and a description of the mean flow solution that is to be used. In Sec. III, the governing equations are presented and decomposed into mean and time-dependent sets. Section IV deals with the temporal set, which is further broken down into an acoustic and a vortical component. The pressure-driven response is dealt with immediately, while the rotational component is left to be evaluated in Sec. V. There, an exact solution to the vortical momentum equation is derived, following a Liouville–Green transformation. The attainment of the vortical set completes the solution for the oscillatory velocity which is described in Sec. VI.

II. DEFINING THE BASIC FLOW MODEL

A. The porous channel

To begin, we consider a long slender channel with porous walls that are separated by a distance $2h$. Therein, fluid is withdrawn from the porous surfaces at a uniform wall velocity v_w. Having defined the length and width of the channel as L and w, we make the assumption of a two-dimensional planar flow by imposing the condition $w\gg h$. In fact, Terrill has shown that when $w/h\geqslant 8$, the presence of lateral walls can be ignored. The system can be further simplified by imposing the condition of symmetry about the channel's midsection plane. This enables us to reduce the solution domain to one half its original size. By way of illustration, a cross section of the channel is shown in Fig. 1. For a symmetric low aspect ratio channel, one can ignore variations in the z direction and reduce the solution domain to $0\leqslant x\leqslant l$, and $0\leqslant y\leqslant 1$, where $l=L/h$ is the dimensionless channel length.

Under the influence of small variations in the suction rate, a channel that is rigid at the head end and isobarically open at the aft end can develop longitudinal pressure oscillations of amplitude A. The corresponding acoustic frequency is specified by

$$\omega_s=(m-\tfrac{1}{2})\pi a_s/L, \tag{1}$$

where a_s refers to the stagnation speed of sound, and m is the oscillation mode number.

B. Limiting conditions

In order to simplify the analysis to the point where an analytical solution can be attempted, several restrictions must be observed. First, the mean flow is assumed to be laminar. The mechanisms of mixing, swirling, or turbulence are also discounted. Constant thermostatic properties are used, and the oscillatory pressure amplitude is taken to be small in comparison with the stagnation pressure. The Mach number, defined as $M\equiv v_w/a_s$, is taken to be a small parameter by imposing the condition $M\ll 1$. Finally, owing to the fact that the mean flow is obtained for an infinitely large Reynolds number, our solutions are limited to $20\leqslant R<\infty$.

C. The steady Sellars flow

The mean flow solution can be obtained by employing the similarity parameter suggested by Berman.[2] In the absence of small amplitude pressure disturbances, the Navier–Stokes equations can be solved exactly through the use of the steady stream function

$$\Psi=-xF(y). \tag{2}$$

Defining $\mathbf{u}_0=(u_0,v_0)$ to be the mean velocity vector normalized by v_w, one can express the components of $\mathbf{u}_0$ as $(u_0,v_0)=(-xF',F)$. The separable component F must satisfy Berman's equation[2]

$$F^{iv}+R(F'F''-FF''')=0, \tag{3}$$

with

$$F'(0)=F(1)=F''(1)=0, \quad F(0)=-1. \tag{4}$$

For a study concerned with large suction, we consider the case investigated by Sellars,[4] Terrill,[5] and Zaturska, Drazin, and Banks,[8] for which

$$\begin{aligned}F(y)&=\frac{R(y-1)-e^{-R}[e^{-R(1-y)}-1]+\frac{1}{2}R^2e^{-R}(y-1)(y-3)+e^{-R}}{R-1+(-\frac{1}{2}R^2+1)e^{-R}}\\&=(y-1)(1+R^{-1})+\tfrac{1}{2}[R^2+(R+1)(y-3)-2]e^{-R}(y-1)-(R^{-1}+R^{-2})e^{-R}[e^{-R(1-y)}-1]+\cdots\\&=y-1+\mathcal{O}(R^{-1}).\end{aligned} \tag{5}$$

Clearly, the basic solution $F=y-1$ proves to be exact for $R\to\infty$. With this choice of F, the velocity and vorticity fields can be written as

$$\mathbf{u}_0=(-x,y-1), \quad \nabla\times\mathbf{u}_0=0. \tag{6}$$

Note that, at leading order, satisfaction of the no-slip condition at the wall is no longer a requirement for the mean flow. This can be attributed to the fact that the mean flow for large suction is insensitive to viscosity. Thus, whereas viscous dissipation will be later shown to play a key role in prescribing the weakly oscillatory flow behavior, its influence on the bulk fluid motion is negligible. Mathematically, dropping the no-slip condition is justified because Berman's equation given by (3) becomes a third-order differential equation (i.e., $F'F''-FF'''=0$) when $R\to\infty$. As such, only three of the four boundary conditions in (4) will be needed. The no-slip condition must be relaxed since the mean flow is no longer constrained by friction at the wall. It is suppressed in order to be consistent with the basic mean flow character that cannot be influenced by shear forces at the wall.

After normalizing the mean pressure by γp_s, (where γ is the ratio of specific heats, and p_s is the stagnation pressure), the complete momentum equation becomes

$$\begin{aligned}&M^2\mathbf{u}_0\cdot\nabla\mathbf{u}_0\\&\quad=-\nabla p_0+R^{-1}[4\nabla(\nabla\cdot\mathbf{u}_0)/3-\nabla\times(\nabla\times\mathbf{u}_0)],\end{aligned} \tag{7}$$

wherefrom

$$p_0=\gamma^{-1}-\tfrac{1}{2}M^2[x^2+(y-1)^2]. \tag{8}$$

III. GOVERNING EQUATIONS

A. Normalized Navier–Stokes

In order to express the differential conservation laws, we evoke dimensionless parameters and see that spatial coordinates are normalized by h, the total instantaneous velocity by a_s, and time by the system's oscillation frequency ω_s. Employing asterisks to represent dimensional variables, spatial and temporal coordinates, velocity, pressure and density can be set as

$$\begin{aligned}&x=x^*/h, \quad y=y^*/h, \quad t=\omega_s t^*, \quad \mathbf{u}=\mathbf{u}^*/a_s,\\&p=p^*/\gamma p_s \text{ and } \rho=\rho^*/\rho_s,\end{aligned} \tag{9}$$

where ρ_s is the stagnation density. Following this choice, the equations of continuity and motion can be expressed in the nondimensional form

$$\omega\partial\rho/\partial t+\nabla\cdot(\rho\mathbf{u})=0, \tag{10}$$

$$\rho[\omega\partial\mathbf{u}/\partial t+(\mathbf{u}\cdot\nabla)\mathbf{u}]$$
$$=-\nabla p+M\varepsilon[4\nabla(\nabla\cdot\mathbf{u})/3-\nabla\times(\nabla\times\mathbf{u})]. \quad (11)$$

Equations (10) and (11) follow the definitions of the nondimensional frequency $\omega\equiv\omega_s h/a_s$, the suction Mach number $M\equiv v_w/a_s$, and the small parameter $\varepsilon\equiv 1/R$.

B. Perturbed variables

With the introduction of small amplitude oscillations at a frequency ω_s, the instantaneous pressure can be expressed as the linear sum of the time-dependent and steady components

$$p(x,y,t)=1/\gamma+\bar{\varepsilon}p_1(x,y)\exp(-it)+\mathcal{O}(M^2x^2), \quad (12)$$

where $i=\sqrt{-1}$, and $\bar{\varepsilon}=A/(\gamma p_s)$ is the pressure wave amplitude. Expressing the density in the same manner, one gets

$$\rho(x,y,t)=1+\bar{\varepsilon}\rho_1(x,y)\exp(-it). \quad (13)$$

Following Lighthill in the assumption of small oscillations,[13] the total velocity can be expanded as

$$\mathbf{u}(x,y,t)=M\mathbf{u}_0(x,y)+\bar{\varepsilon}\mathbf{u}_1(x,y)\exp(-it). \quad (14)$$

C. Total field decomposition

Equations (12)–(14) must be inserted back into Eqs. (10) and (11). The zero-order terms yield the mean flow equations. Likewise, $\mathcal{O}(\bar{\varepsilon})$ terms result in

$$-i\omega\rho_1+\nabla\cdot\mathbf{u}_1=-M\nabla\cdot(\rho_1\mathbf{u}_0), \quad (15)$$

$$-i\omega\mathbf{u}_1=-M[\nabla(\mathbf{u}_0\cdot\mathbf{u}_1)-\mathbf{u}_1\times(\nabla\times\mathbf{u}_0)$$
$$-\mathbf{u}_0\times(\nabla\times\mathbf{u}_1)]-\nabla p_1+M\varepsilon[4\nabla(\nabla\cdot\mathbf{u}_1)/3$$
$$-\nabla\times(\nabla\times\mathbf{u}_1)]. \quad (16)$$

Equations (15) and (16) describe the intimate coupling between mean and steady motions. They clearly indicate that the mean velocity $\mathbf{u}_0$ has a strong influence on the oscillatory flow component $\mathbf{u}_1$.

IV. TEMPORAL FIELD DECOMPOSITION

A. Irrotational and solenoidal vectors

In order to further proceed, the temporal disturbances are split into solenoidal and irrotational components. Using a circumflex to denote the curl-free pressure-driven part, and a tilde for the divergence-free boundary-driven part, the time-dependent velocity component can be expressed as

$$\mathbf{u}_1=\hat{\mathbf{u}}+\tilde{\mathbf{u}}, \quad (17)$$

with

$$\boldsymbol{\Omega}_1=\nabla\times\mathbf{u}_1=\nabla\times\tilde{\mathbf{u}}, \quad p_1=\hat{p}, \quad \rho_1=\hat{\rho}. \quad (18)$$

This decomposition charges all vortices to the solenoidal field, and compressibility sources and sinks to the irrotational field. Such decomposition is based on a fundamental theorem of vector analysis that was first addressed by Stokes[14] in 1849 and then proven rigorously by Blumenthal in 1905. Furthermore, the celebrated theorem appears to be at the root of Helmholtz's work on vortex motion in 1858.

B. The linearized Navier–Stokes equations

Insertion of Eqs. (17) and (18) into Eqs. (15) and (16) leads to two independent sets that are only coupled through existing boundary conditions. One set that we call acoustic is compressible and irrotational; the other, we call vortical, is incompressible and rotational. These responses are byproducts of pressure-driven and vorticity-driven oscillation modes at $\mathcal{O}(\bar{\varepsilon})$.

1. The acoustic set

$$-i\omega\hat{\rho}+\nabla\cdot\hat{\mathbf{u}}=-M\nabla\cdot(\hat{\rho}\mathbf{u}_0), \quad (19)$$

$$-i\omega\hat{\mathbf{u}}=-\nabla\hat{p}+4M\varepsilon\nabla(\nabla\cdot\hat{\mathbf{u}})/3-M[\nabla(\hat{\mathbf{u}}\cdot\mathbf{u}_0)$$
$$-\hat{\mathbf{u}}\times(\nabla\times\mathbf{u}_0)]. \quad (20)$$

2. The vortical set

$$\nabla\cdot\tilde{\mathbf{u}}=0, \quad (21)$$

$$-i\omega\tilde{\mathbf{u}}=-M\varepsilon\nabla\times(\nabla\times\tilde{\mathbf{u}})-M[\nabla(\tilde{\mathbf{u}}\cdot\mathbf{u}_0)-\tilde{\mathbf{u}}\times(\nabla\times\mathbf{u}_0)$$
$$-\mathbf{u}_0\times(\nabla\times\tilde{\mathbf{u}})]. \quad (22)$$

C. Boundary conditions

Unlike the basic mean flow solution that does not produce any vorticity, the rotationality that accompanies the small time-dependent fluctuations is susceptible to viscous dissipation. The strong sensitivity to viscosity must therefore be accounted for by insuring that friction at the wall is felt by temporal oscillations. In fact, without friction at the wall, no unsteady vorticity can be generated. At the outset, one realizes that the two boundary conditions that must be satisfied by the unsteady velocity component $\mathbf{u}_1$ have to be the same as those used in the injection-flow analogue;[15,16] namely, the no-slip condition at the wall $u_1(x,0)=0$, and symmetry about the midsection plane, $\partial u_1(x,1)/\partial y=0$. In principle, these conditions must be observed whenever symmetric mean flow solutions are used to represent the bulk fluid motion.

D. Acoustic solution

Assuming, as usual,[17] isentropic pressure oscillations, the linearization process yields $\hat{p}=\hat{\rho}$. In order to recognize that $\hat{p}=\hat{\rho}$, it is useful to recall the fundamental isentropic relation, $p^*/p_s=(\rho^*/\rho_s)^\gamma$. Following Eqs. (12) and (13), one can write

$$p^*=p_s+Ap_1(x,y)\exp(-it),$$
$$\rho^*=\rho_s[1+\bar{\varepsilon}\rho_1(x,y)\exp(-it)], \quad (23)$$

where $\bar{\varepsilon}=A/(\gamma p_s)$ is the dimensionless pressure wave amplitude. Substitution of the expanded variables into the isentropic relation yields

$$\frac{p_s+Ap_1(x,y)\exp(-it)}{\gamma p_s}=\frac{1}{\gamma}\left\{\frac{\rho_s[1+\bar{\varepsilon}\rho_1(x,y)\exp(-it)]}{\rho_s}\right\}^\gamma, \quad (24)$$

where both sides have been divided by γ. At this point, it is clear that

$$\gamma^{-1}+\overline{\varepsilon}p_1\exp(-it)=\gamma^{-1}[1+\overline{\varepsilon}\rho_1\exp(-it)]^{\gamma}$$
$$=\gamma^{-1}[1+\gamma\overline{\varepsilon}\rho_1\exp(-it)+\gamma(\gamma-1)\overline{\varepsilon}^2\rho_1^2\exp(-2it)/2!+\cdots], \quad (25)$$

where the binomial formula has been used to expand the right-hand side. Truncating the series at $\mathcal{O}(\overline{\varepsilon}^2)$ gives $p_1=\rho_1$ and, from Eq. (18), $\hat{p}=\hat{\rho}$. This is so because the pseudopressure and density arising from the rotational solution are of second order in the wave amplitude.[12]

At this juncture, one can multiply Eq. (19) by $-i\omega$, take the divergence of Eq. (20), and combine the resulting terms; a wave equation is produced, namely

$$\nabla^2\hat{p}+\omega^2\hat{p}=4M\varepsilon\nabla^2(\nabla\cdot\hat{\mathbf{u}})/3-M\{i\omega\nabla\cdot(\mathbf{u}_0\hat{p})+\nabla^2(\hat{\mathbf{u}}\cdot\mathbf{u}_0)-\nabla\cdot[\hat{\mathbf{u}}\times(\nabla\times\mathbf{u}_0)]\}. \quad (26)$$

A solution at $\mathcal{O}(M)$ can be achieved through the use of separation of variables. This solution, corresponding to longitudinal oscillations, proceeds from the rigid wall boundary conditions. At the outset, the acoustic pressure and velocity become

$$\hat{p}=\cos(\omega x)+\mathcal{O}(M), \quad \hat{\mathbf{u}}=i\sin(\omega x)\hat{\mathbf{i}}+\mathcal{O}(M). \quad (27)$$

E. Vortical equations

Assuming that the ratio of the normal to the x-component of the velocity is of the same order as the Mach number (i.e., $\tilde{v}/\tilde{u}=\mathcal{O}(M)$), $\tilde{v}$ can be neglected. This assumption can be justified in view of the arguments presented by Flandro[18] and Majdalani and Van Moorhem.[1] Applying this condition, along with the definition of the mean flow velocity, the x-component of the momentum equation reduces to

$$iSr\tilde{u}=\frac{\partial}{\partial x}(\tilde{u}u_0)+v_0\frac{\partial\tilde{u}}{\partial y}-\varepsilon\frac{\partial^2\tilde{u}}{\partial y^2}+\mathcal{O}(M), \quad (28)$$

where $Sr\equiv\omega/M$ is the Strouhal number. For large suction, Eq. (28) becomes

$$iSr\tilde{u}=(y-1)\frac{\partial\tilde{u}}{\partial y}-x\frac{\partial\tilde{u}}{\partial x}-\tilde{u}-\varepsilon\frac{\partial^2\tilde{u}}{\partial y^2}+\mathcal{O}(M). \quad (29)$$

An exact solution to Eq. (29) is presented next.

V. THE EXACT SOLENOIDAL SOLUTION

A. The separable boundary-layer equation

An exact solution to Eq. (29) can be achieved through the use of separation of variables. Assuming the form

$$\tilde{u}(x,y)=X(x)Y(y), \quad (30)$$

substitution into Eq. (29) leads to

$$\frac{x}{X}\frac{dX}{dx}=\frac{(y-1)}{Y}\frac{dY}{dy}-\frac{\varepsilon}{Y}\frac{d^2Y}{dy^2}-iSr-1=\kappa_n, \quad (31)$$

where $\kappa_n>0$ is the separation eigenvalue. Integration of the x-equation can be performed easily and then inserted into Eq. (30). The solution becomes

$$\tilde{u}(x,y)=\sum_n c_n x^{\kappa_n}Y_n(y), \quad (32)$$

where c_n is an integration constant associated with κ_n. Satisfaction of the no-slip boundary condition at the wall requires setting the acoustic and vortical velocity components equal and opposite at $y=0$. One finds

$$\tilde{u}(x,0)=-i\sin(\omega x). \quad (33)$$

Using a series expansion of the sine function, and setting the result equal to Eq. (32), one gets

$$\sum_n c_n x^{\kappa_n}Y_n(0)=-i\sum_{n=0}^{\infty}\frac{(-1)^n(\omega x)^{2n+1}}{(2n+1)!}. \quad (34)$$

Equating terms yields

$$\kappa_n=2n+1, \quad c_n=-i\frac{(-1)^n\omega^{2n+1}}{(2n+1)!}, \quad Y_n(0)=1, \quad (35)$$

where $n=0,1,2,...,\infty$. The expression for the rotational component becomes

$$\tilde{u}(x,y)=-i\sum_{n=0}^{\infty}\frac{(-1)^n(\omega x)^{2n+1}}{(2n+1)!}Y_n. \quad (36)$$

In order to complete Eq. (36), Y_n needs to be determined from Eq. (31). The search for Y_n leads to a boundary-value problem of the form

$$\varepsilon\frac{d^2Y_n}{dy^2}-(y-1)\frac{dY_n}{dy}+(iSr+2n+2)Y_n=0, \quad (37)$$

that is subject to

$$Y_n(0)=1, \quad Y_n'(1)=0. \quad (38)$$

The two boundary conditions stem from the no-slip and core symmetry requirements.

B. The Liouville–Green transformation

Careful examination of Eq. (37) leads us to believe that an exact solution is tractable if the equation is first transformed from a variable coefficient ODE, to an equation with constant coefficients. Working toward that end, the Liouville–Green transformation is applied by first setting $r=1-y$. This transforms Eq. (37) into

$$\varepsilon\frac{d^2Y_n}{dr^2}-r\frac{dY_n}{dr}+(iSr+2n+2)Y_n=0, \quad (39)$$

with boundary conditions $Y_n(1)=1$ and $Y_n'(0)=0$. Next, we define

$$Z=\phi(r), \quad B(Z)=\psi(r)Y_n(r). \quad (40)$$

These change the derivatives of Y_n into

$$\frac{dY_n}{dr}=-\frac{\psi'}{\psi^2}B+\frac{1}{\psi}\frac{dB}{dZ}\frac{dZ}{dr}=-\frac{\psi'}{\psi^2}B+\frac{\phi'}{\psi}\frac{dB}{dZ}, \quad (41)$$

$$\frac{d^2Y_n}{dr^2}=\frac{\phi'^2}{\psi}\frac{d^2B}{dZ^2}+\left(\frac{\phi''}{\psi}-\frac{2\phi'\psi'}{\psi^2}\right)\frac{dB}{dZ}-\left(\frac{\psi''}{\psi^2}-\frac{2\psi'^2}{\psi^3}\right)B, \quad (42)$$

where primes stand for differentiation with respect to r. Substitution of these derivatives into Eq. (39) gives

$$\frac{d^2B}{dZ^2}+\frac{1}{\phi'^2}\left(\phi''-\frac{2\phi'\psi'}{\psi}-rR\phi'\right)\frac{dB}{dZ}+\frac{1}{\phi'^2}\left(-\frac{\psi''}{\psi}+\frac{2\psi'^2}{\psi^2}+\frac{rR\psi'}{\psi}\right)B+\frac{R}{\phi'^2}(iSr+2n+2)B=0. \tag{43}$$

The functions ψ and ϕ are now chosen to force the variable coefficients in the transformed equation to be constant values. To do this, the coefficient of the first derivative term is set equal to zero; hence

$$\psi'/\psi=(\phi''/\phi'-rR)/2. \tag{44}$$

Integrating gives $\psi=H_0\sqrt{\phi'}\exp(-Rr^2/4)$, where H_0 is a subsidiary constant. Equation (43) simplifies into

$$\frac{d^2B}{dZ^2}+\left\{\frac{R}{\phi'^2}(iSr-2n+2)+\delta\right\}B=0, \tag{45}$$

where

$$\delta=\frac{1}{\phi'^2}\left(-\frac{\psi''}{\psi}+\frac{2\psi'^2}{\psi^2}+\frac{rR\psi'}{\psi}\right). \tag{46}$$

By imposing

$$\frac{R}{\phi'^2}[iSr+(2n+2)]=\text{constant}, \tag{47}$$

one obtains

$$\phi'=\sqrt{R}\ \text{ and }\ Z=\phi=r\sqrt{R}. \tag{48}$$

Furthermore, setting $H_0=1/\sqrt[4]{R}$ gives

$$\psi(r)=\exp(-Rr^2/4). \tag{49}$$

Finally, the transformed equation and corresponding boundary conditions become

$$\frac{d^2B}{dZ^2}+(p+\tfrac{1}{2}-\tfrac{1}{4}Z^2)B=0;\ \ p=2+2n+iSr, \tag{50}$$

with

$$B(\sqrt{R})=\exp(-R/4);\ \ \frac{dB(0)}{dZ}=0. \tag{51}$$

C. The complete solution

Equation (50) is a Weber differential equation. This type is known to have independent solutions that are parabolic cylinder functions of the form

$$B(Z)=K_1D_p(Z)+K_2D_p(-Z). \tag{52}$$

Due to the complexity of the parabolic cylinder functions, symbolic programming may be relied upon to evaluate the constants K_1 and K_2. This is done in fulfillment of the boundary conditions given by Eq. (51). The result is

$$K_1=K_2=2^{-1-p/2}\Gamma(\tfrac{1}{2}-\tfrac{1}{2}p)/[\sqrt{\pi}\Phi(-\tfrac{1}{2}p,\tfrac{1}{2},\tfrac{1}{2}R)], \tag{53}$$

where Γ is Euler's Gamma function and Φ is the confluent hypergeometric function. The latter is expandable in a series of the type

$$\Phi(a,b;x)=1+\frac{a}{b}\frac{x}{1!}+\frac{a(a+1)}{b(b+1)}\frac{x^2}{2!}+\frac{a(a+1)(a+2)}{b(b+1)(b+2)}\frac{x^3}{3!}+\cdots. \tag{54}$$

Substitution of Eqs. (52) and (53) into Eq. (40) leads to

$$Y_n(r)=\frac{\Phi(-\tfrac{1}{2}p,\tfrac{1}{2},\tfrac{1}{2}Rr^2)}{\Phi(-\tfrac{1}{2}p,\tfrac{1}{2},\tfrac{1}{2},R)}. \tag{55}$$

One may now revert back to original variables and revisit Eq. (36). One finds

$$\tilde{u}=-i\sum_{n=0}^{\infty}\frac{(-1)^n(\omega x)^{2n+1}\Phi[-\tfrac{1}{2}p,\tfrac{1}{2},\tfrac{1}{2}R(y-1)^2]}{(2n+1)!\Phi(-\tfrac{1}{2}p,\tfrac{1}{2},\tfrac{1}{2}R)}. \tag{56}$$

Using continuity, the normal component of the rotational velocity can be deduced also. From Eq. (21) we have

$$\tilde{v}=-\int\frac{\partial\tilde{u}}{\partial x}dy=-i\omega r\sum_{n=0}^{\infty}\frac{(-1)^n(\omega x)^{2n}\Phi(-\tfrac{1}{2}p,\tfrac{3}{2},\tfrac{1}{2}Rr^2)}{(2n)!\Phi(-\tfrac{1}{2}p,\tfrac{1}{2},\tfrac{1}{2}R)}+iA(x), \tag{57}$$

where $A(x)$ is an admittance function that depends on the wall's material properties and porosity. In view of Eqs. (56) and (57), the total oscillatory velocity can now be constructed by summing both acoustical and vortical components. At length, one obtains

$$u_1=i\left[\sin(\omega x)-\sum_{n=0}^{\infty}\frac{(-1)^n(\omega x)^{2n+1}\Phi(a,b,\tfrac{1}{2}RF^2)}{(2n+1)!\Phi(a,b,\tfrac{1}{2}R)}\right], \tag{58}$$

$$v_1=i\omega F\sum_{n=0}^{\infty}\frac{(-1)^n(\omega x)^{2n}\Phi(a,c,\tfrac{1}{2}RF^2)}{(2n)!\Phi(a,b,\tfrac{1}{2}R)}+iA(x), \tag{59}$$

with $a=-1-n-\frac{1}{2}iSr$, $b=1/2$, and $c=3/2$.

D. Numerical verification

The analytical solution that we constructed can be easily verified via comparisons with the numerical solution of Eq. (29). This can be accomplished using the same numerical code that was developed by Majdalani and Van Moorhem[1] for the injection case. For large suction, we obtain a uniform agreement of at least six significant digits using a step size of $\Delta y=5\times10^{-6}$. Note that, for injection, numerical predictions acquired by the same code were shown, in previous studies,[1,19] to agree with both asymptotic and experimental observations.

Comparing the numerical output to the asymptotic solution of the linearized momentum equation [Eq. (29)] serves a

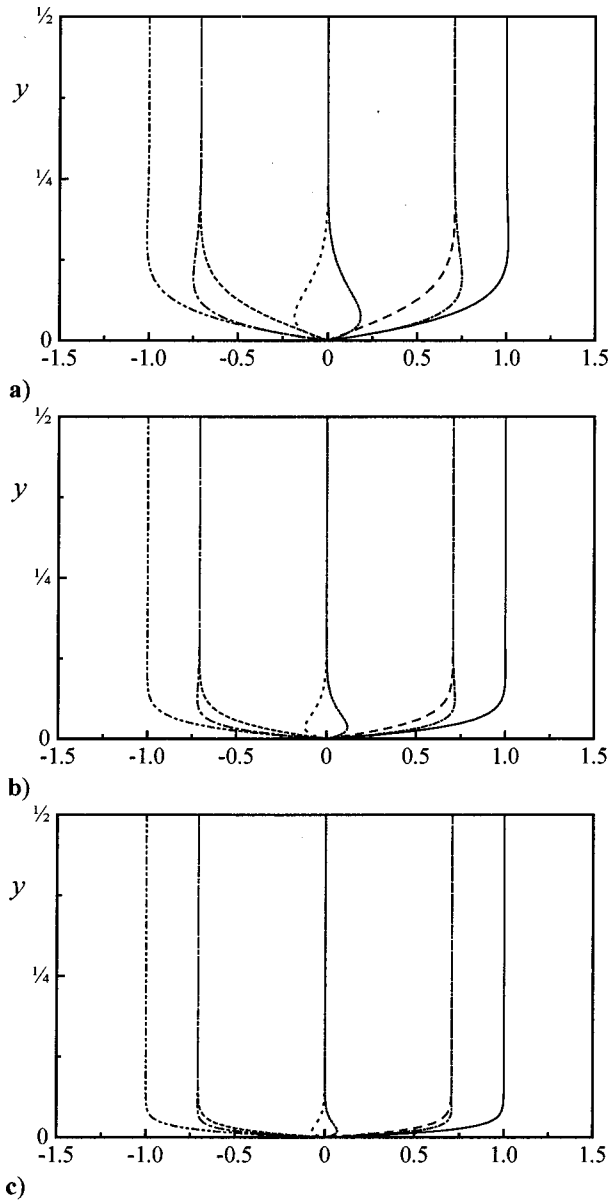

FIG. 2. The oscillatory velocity $u_1 \exp(-it)$ plotted at eight different times for $m=1$, $x/l=1$, $Sr=20$, and (a) $R=20$, (b) $R=50$, and (c) $R=100$. This variation can be due to a progressive decrease in viscosity. Here t corresponds to —— 0°, – – – – 45°, - - - - 90°, –-–-–-– 135°, –––––– 180°, ---- 225°, ···· 270°, –·–·–· 315°, —— 360°.

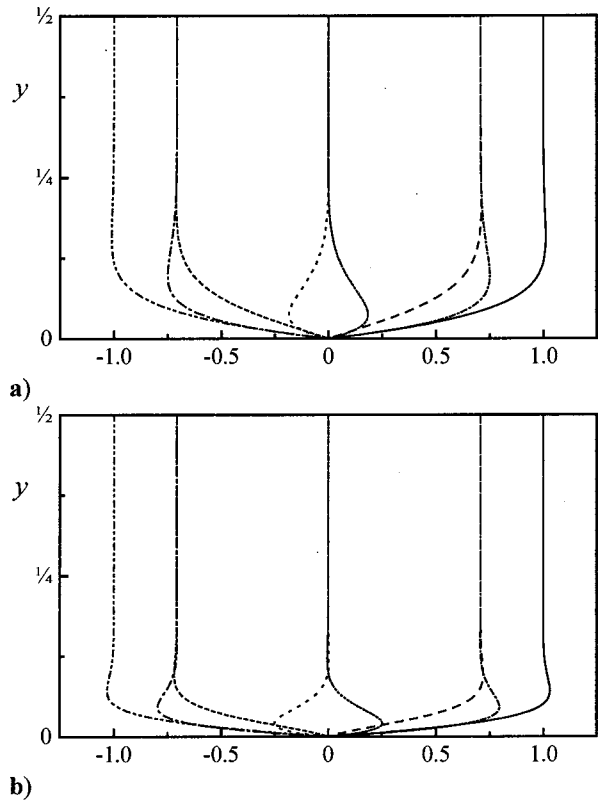

FIG. 3. The oscillatory velocity $u_1 \exp(-it)$ plotted at eight different times for $x/l=1$, $R=20$, and $m=1$. Properties correspond to (a) $Sr=10$ and (b) $Sr=100$. This variation is due to an order of magnitude increase in oscillation frequency. Higher Sr increase the overshoot while reducing the penetration depth. Here t corresponds to —— 0°, – – – – 45°, - - - - 90°, –-–-–-– 135°, –––––– 180°, ---- 225°, ···· 270°, –·–·–· 315°, —— 360°.

dual purpose. First, it increases our confidence in the numerical algorithm that we used to integrate the momentum equation. Second, it insures the correctness of the procedure that led to the exact solution.

VI. DISCUSSION

Based on Eq. (58), the time evolution of the x-component of the velocity is analyzed in Figs. 2–4 over a range of parameters. At first glance, the profiles seem to concur with the classic theory of time-dependent flows. In particular, the reader is referred to the fairly well-presented survey by Rott.[20] On that account, a strong resemblance is found between our solution and the oscillatory flow solution over nonpermeable walls. In both cases, the velocity appears to be a traveling wave with two distinct components. A viscous, rotational component that is dominant near the wall, and an inviscid, acoustic part that is retained near the core. While their sum satisfies the no slip at the wall, the rotational part decays as the distance from the wall is increased. The rotational layer and corresponding thickness appear to be largest for relatively small values of the suction Reynolds number. The profile also exhibits a small velocity overshoot near the wall. This phenomenon is known as Richardson's annular effect and is a characteristic of oscillatory flows.[21] It can take place near the wall when rotational and acoustic waves have favorable phases and, hence, additive amplitudes.

In order to illustrate the effect of R on the solution, the suction Reynolds number is increased in Fig. 2 by one order of magnitude while keeping other variables constant. As the Reynolds number is increased, viscous effects become less pronounced: The penetration depth (i.e., rotational boundary-layer) becomes smaller. The Richardson overshoot also diminishes. This effect is to be expected because the convective withdrawal at the wall becomes more appreciable with successive increases in R. Clearly, suction seems to inhibit the boundary-layer growth near the wall. This effect is contrary to what has been reported in the presence of injection. As shown by Majdalani[15,16] increasing injection increases the

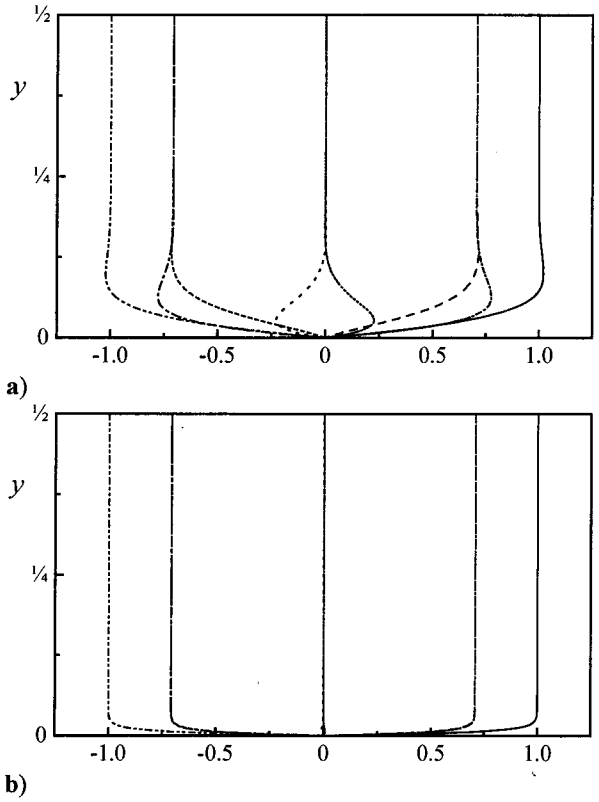

FIG. 4. The oscillatory velocity $u_1 \exp(-it)$ plotted at eight different times for $x/l=1$, and $m=1$. Properties correspond to (a) $R=20$, $Sr=50$, and (b) $R=200$, $Sr=5$. This variation is due to an order of magnitude increase in suction speed. Clearly, large suction reduces both penetration depth and overshoot. Here t correspond to —— 0°, – – – – 45°, - - - - 90°, –-–-–-– 135°, –––––– 180°, ---- 225°, ···· 270°, –·–·–· 315°, —— 360°.

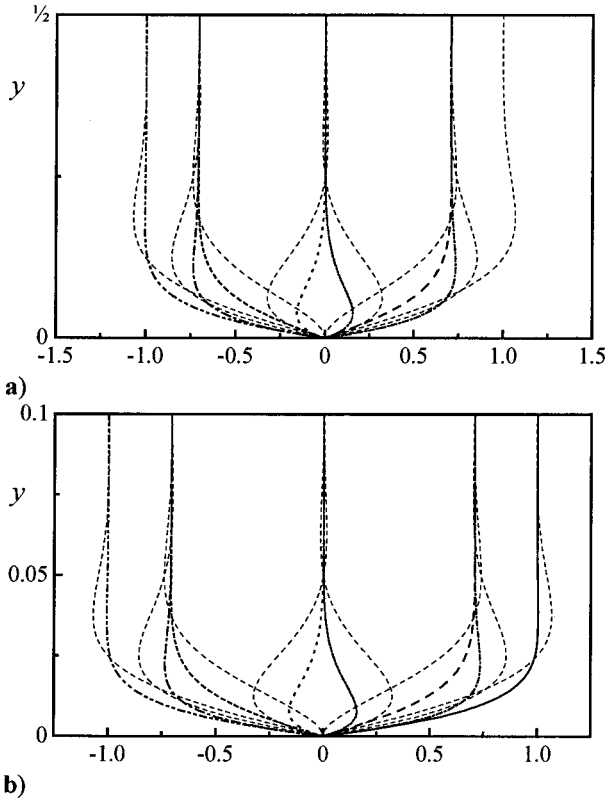

FIG. 5. Comparison between the oscillatory velocities with and without suction. Both $u_1 \exp(-it)$ and the exact Stokes solution (over hard walls) are shown at eight different times for $x/l=1$, $v_w=2^{1/6}\sqrt{\omega_s \nu}$, and $m=1$. Parameters are: (a) $R=20$, $Sr=16$, and (b) $R=100$, $Sr=80$. The suction speed is set below the small Stokes diffusion speed. Timelines show that the penetration depth and overshoot are reduced with suction. Here t corresponds to —— 0°, – – – – 45°, - - - - 90°, –-–-–-– 135°, –––––– 180°, ---- 225°, ···· 270°, –·–·–· 315°, —— 360°.

penetration depth. Injection also leads to a substantially larger velocity overshoot.

In Fig. 3, the effect of varying the oscillation frequency is captured. Thus, as the Strouhal number is increased from 10 to 100, a slight increase in the Richardson effect is noted. This is accompanied by a reduction in penetration depth. Our observation indicates a consistency with the effect of varying frequency in the presence of injection. In both cases, increasing frequency increases the temporal velocity near the wall and decreases the penetration depth. The increased overshoot can be attributed to the fact that the normal rotational wavelength is inversely proportional to Sr. A shorter wavelength leads, of course, to a vortico-acoustic coupling that is closer to the wall. Since the vortical amplitude increases as we draw nearer to the wall, a larger vortical contribution can be added to the acoustic component at shorter wavelengths. This additional contribution is responsible for the increased overshoot.

In Fig. 4, all parameters are fixed except for the suction speed. Hence, as v_w is increased by one order of magnitude, a reduction in penetration depth and breadth (overshoot) are noted. The influence of suction speed on altering the flow character is certainly the greatest. Surveying these figures as a whole suggests that, over a wide range of Reynolds and Strouhal numbers, the boundary layer at the wall shares several similarities with the classic Stokes layer over hard walls. As opposed to the penetration depth with injection, the suction boundary layer here is much thinner. The velocity overshoot is also minimal. These characteristics are markedly different from the basic features of an oscillatory flow with wall injection.[15,16]

In order to compare our solution directly to the exact solution by Stokes, the suction speed is reduced to a value below the Stokes diffusion speed, $\sqrt{2\omega_s \nu}$. Letting $v_w = 2^{1/6}\sqrt{\omega_s \nu}$, the Stokes number becomes

$$h\sqrt{\omega_s/2\nu} = Sr^2/R. \tag{60}$$

For this particular condition, one can compare in Fig. 5 the current asymptotic solution to the Stokes exact profile for oscillations in a channel with hard walls. In the interest of clarity, the Stokes profile is expressed in our nomenclature and written as

$$u_1 \exp(-it) = \sin(t) - \exp[\sqrt{SrR/2}(y-1)] \times \sin[t+\sqrt{SrR/2}(y-1)]. \tag{61}$$

As shown at two different Reynolds numbers, the presence of suction attracts the shear layers closer to the wall. As a result, both rotational depth and overshoot are reduced when

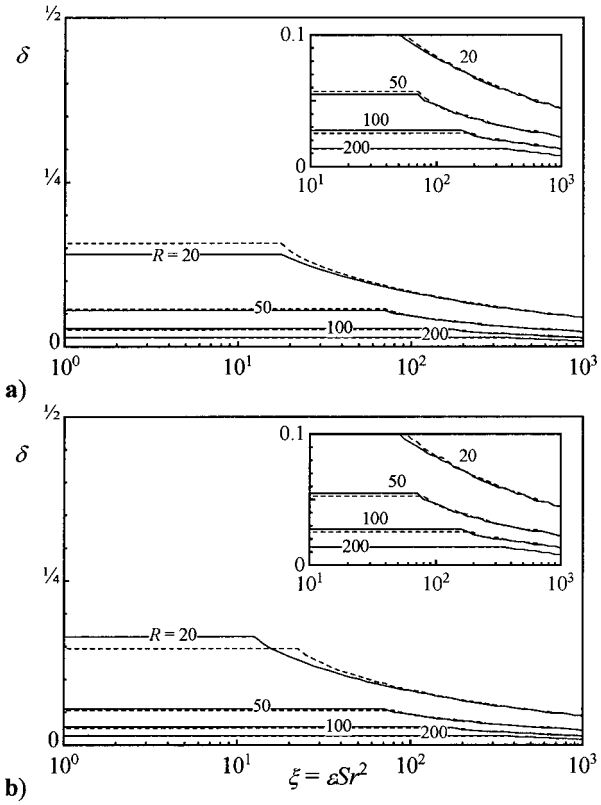

FIG. 6. Boundary-layer thickness versus the viscous parameter for a Reynolds number ranging between $R=20$ and $R=200$ at (a) $m=1$ and (b) $m=2$. The penetration depth is seen to decrease with increases in both Reynolds number and Strouhal number. In addition, some axial dependence on boundary-layer thickness is noted. Solid and broken lines correspond to $x/l=$—— 0.01, ------ 0.99.

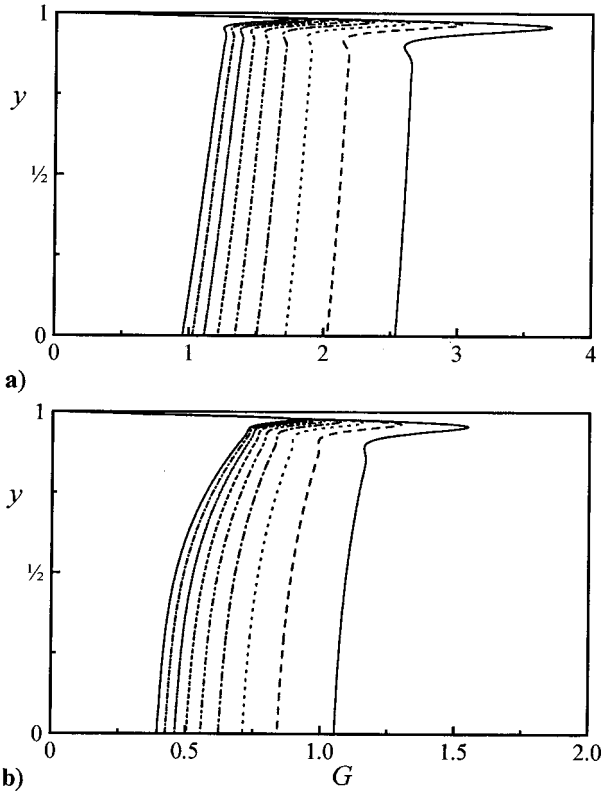

FIG. 7. Plots of $G=\tilde{v}/(M\tilde{u})$ versus y for $Sr=50$ and $m=1$ at various Reynolds numbers. Axial positions correspond to (a) $x/l=0.25$, and (b) $x/l=0.5$. Results support the assumption that $\tilde{v}/\tilde{u}=\mathcal{O}(M)$. Suction Reynolds numbers correspond to: —— 100; -·-·-·-·- 90; ------ 80; - - - - - - 70; -·-·-·-·- 60; -·-·-·-·- 50; - - - - - - 40; - - - - - - 30; —— 20.

suction is present. The boundary-layer thickness with suction is thus thinner than the traditional Stokes layer.

In Fig. 6, the penetration depth δ is plotted versus the viscous parameter $\xi=\varepsilon Sr^2=\nu\omega_s^2 h v_w^{-3}$ at axial locations corresponding to the fore and aft ends of the channel. The Reynolds and Strouhal numbers are varied throughout the range of physical parameters under consideration, and the resulting figures again show that the penetration depth decreases with an increase in either R or ξ. Comparing the thickness of the penetration depth at the extreme axial locations indicates that the axial dependence of δ is small at relatively low suction levels and insignificant when suction is increased. This spatial dependence becomes less appreciable when the viscous parameter is increased. The role of viscosity as an inhibitor of rotational growth is consistent with our analysis of the oscillatory velocity. It is clear from Fig. 6 that δ becomes smaller when either the viscosity or frequency are increased. Moreover, the penetration depth appears to be a weak function of the oscillation mode number.

In closing, we use Fig. 7 to verify the assumption made earlier to simplify the vorticity-driven momentum equation into a form that is susceptible to an exact solution. To that end, one may recall that our decomposition of the time-dependent equations required $\tilde{v}/\tilde{u}$ to be of the same order as that of the wall suction Mach number. This assumption can be substantiated by defining $G=\tilde{v}/(\tilde{u}M)$ and later verifying that $G\sim\mathcal{O}(1)$. This is indeed accomplished in Fig. 7 where G is evaluated at several axial locations. Clearly, the magnitude of G increases as we move toward the head end. Despite this spatial dependence, G appears to be of $\mathcal{O}(1)$ throughout the channel length. Being the outcome of an exact solenoidal solution, this result indicates that our assumption of $\tilde{v}/\tilde{u}\sim\mathcal{O}(M)$ used in Sec. IV E was justifiable.

[1] J. Majdalani and W. K. Van Moorhem, "Improved time-dependent flowfield solution for solid rocket motors," AIAA J. **36**, 241 (1998).
[2] A. S. Berman, "Laminar flow in channels with porous walls," J. Appl. Phys. **24**, 1232 (1953).
[3] S. W. Yuan, "Further investigation of laminar flow in channels with porous walls," J. Appl. Phys. **27**, 267 (1956).
[4] J. R. Sellars, "Laminar flow in channels with porous walls at high suction Reynolds numbers," J. Appl. Phys. **26**, 489 (1955).
[5] R. M. Terrill, "Laminar flow in a uniformly porous channel," Aeronaut. Q. **15**, 299 (1964).
[6] W. A. Robinson, "The existence of multiple solutions for the laminar flow in a uniformly porous channel with suction at both walls," J. Eng. Math. **10**, 23 (1976).
[7] A. D. MacGillivray and C. Lu, "Asymptotic solution of a laminar flow in a porous channel with large suction: A nonlinear turning point problem," Meth. Appl. Anal. **1**, 229 (1994).
[8] M. B. Zaturska, P. G. Drazin, and W. H. H. Banks, "On the flow of a viscous fluid driven along a channel by suction at porous walls," Fluid Dyn. Res. **4**, 151 (1988).
[9] M. B. Zaturska and W. H. H. Banks, "Suction-driven flow in a porous pipe," J. Appl. Math. Mech. (ZAMM) **75**, 21 (1995).

[10]S. M. Cox and A. C. King, ''On the asymptotic solution of a high-order nonlinear ordinary differential equation,'' Proc. R. Soc. London, Ser. A **453**, 711 (1997).
[11]C. Lu, ''On the asymptotic solution of laminar channel flow with large suction,'' SIAM (Soc. Ind. Appl. Math.) J. Math. Anal. **28**, 1113 (1997).
[12]B.-T. Chu and L. S. G. Kovásznay, ''Non-linear interactions in a viscous heat-conducting compressible gas,'' J. Fluid Mech. **3**, 494 (1957).
[13]M. J. Lighthill, ''The response of laminar skin friction and heat transfer to fluctuations in the stream velocity,'' Proc. R. Soc. London, Ser. A **224**, 1 (1954).
[14]G. G. Stokes, ''On the dynamical theory of diffraction,'' Math. and Phys. Papers **2**, 243 (1883).
[15]J. Majdalani, ''The boundary layer structure in cylindrical rocket motors,'' AIAA J. **37**, 505 (1999).
[16]J. Majdalani, ''Asymptotic formulation for an acoustically driven field inside a rectangular cavity with a well-defined convective mean flow motion,'' J. Sound Vib. **223**, 73 (1999).
[17]J. Majdalani and T. S. Roh, ''The oscillatory channel flow with large wall injection,'' Proc. R. Soc. London, Ser. A **456**, 1625 (2000).
[18]G. A. Flandro, ''Effects of vorticity on rocket combustion stability,'' J. Propul. Power **11**, 607 (1995).
[19]J. Majdalani and W. K. Van Moorhem, ''A multiple-scales solution to the acoustic boundary layer in solid rocket motors,'' J. Propul. Power **13**, 186 (1997).
[20]N. Rott, ''Theory of time-dependent laminar flows,'' in *High Speed Aerodynamics and Jet Propulsion—Theory of Laminar Flows*, edited by F. K. Moore (Princeton University Press, Princeton, NJ, 1964), Vol. IV, pp. 395–438.
[21]H. Schlichting, *Boundary-Layer Theory*, 7th ed. (McGraw-Hill, New York, 1979).